Inorganic Chemistry
Article
pubs.acs.org/IC

Structural Properties and Singular Phase Transitions of Metallic $Pr_{0.50}Sr_{0.50}CoO_3$ Cobaltite

Jessica Padilla-Pantoja,[†] José Luis García-Muñoz,*[,†] Bernat Bozzo,[†] Zdeněk Jirák,[‡] and Javier Herrero-Martín[§]

[†]Institut de Ciència de Materials de Barcelona, ICMAB-CSIC, Campus universitari de Bellaterra, E-08193 Bellaterra, Spain
[‡]Institute of Physics, ASCR, Cukrovarnická 10, 162 00 Prague 6, Czech Republic
[§]ALBA Synchrotron, 08290 Cerdanyola del Vallès, Barcelona, Spain

ABSTRACT: The $Pr_{0.50}Sr_{0.50}CoO_3$ perovskite exhibits unique magnetostructural properties among the rest of the ferromagnetic/metallic $Ln_{0.50}Sr_{0.50}CoO_3$ compounds. Existing reports are largely controversial. We have determined and described its structural evolution, which follows the $Pm\bar{3}m \rightarrow R\bar{3}c \rightarrow Imma \rightarrow I4/mcm$ transformations. The structural changes have been thoroughly described. The results are confronted with distinct nonconventional properties and spin–lattice coupling effects in another half-doped cobaltite based on praseodymium, $Pr_{0.50}Ca_{0.50}CoO_3$. The *Imma* → *I*4/*mcm* symmetry change is responsible for the unexpected second magnetic transition.

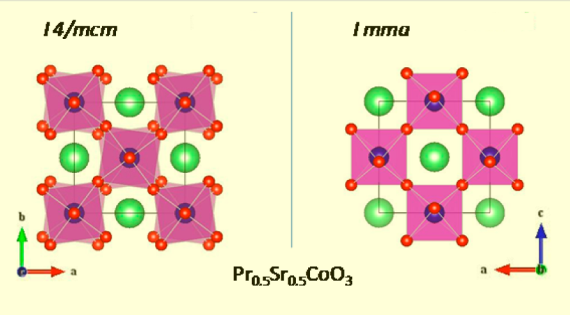

I. INTRODUCTION

Like in the widely studied manganites, the double exchange between Co^{3+} and Co^{4+} species is considered to be an effective mechanism to produce a ferromagnetic (FM)/metallic state in cobaltites. Nevertheless, distinct specific features make these two families exhibit very different physical properties and phase transitions. For instance, the hybridization between 3d metal and 2p O orbitals is more intense in cobalt oxides favoring the delocalization of charges. Covalency effects and hybridization with holes on oxygen states may favor intermediate-spin (IS) and low-spin (LS) states. Such an ability of Co^{3+} and Co^{4+} ions to adopt different spin states is another key feature generating great interest because of the relevance of the spin state of cobalt for electron mobility.[1−7]

In particular, the half-doped $Pr_{0.50}A_{0.50}CoO_3$ (A = Ca or Sr) perovskites with spin–lattice coupling exhibit distinct properties, the interpretation of which has been controversial. $Pr_{0.50}Ca_{0.50}CoO_3$ (PCCO) is metallic but undergoes an unexpected metal–insulator (MIT) and concomitant cobalt spin-state transition at $T_{MI} \sim 80$ K.[8−14] At this temperature, its *Pnma* cell suddenly shrinks because of contraction of some Pr–O bonds that is accompanied by a partial Pr^{3+} to Pr^{4+} valence shift.[9,12,13] As a consequence, the insulating state emerges by electron transfer from praseodymium to cobalt sites and stabilization of the Co^{3+} LS state.[11−14] The loss of the magnetic moment due to the large fraction of cobalt sites with $S = 0$ at $T < T_{MI}$ prevents spontaneous long-range FM order, although this can be easily induced under a magnetic field.

$Pr_{0.50}Sr_{0.50}CoO_3$ (PSCO) is metallic down to low temperatures and exhibits FM order below $T_C \sim 230$ K, originated in the double-exchange interactions. In addition, Mahendiran and Schiffer reported a second unexpected transition at $T \sim 120$ K characterized by a drop of the magnetization.[15] Such two-step magnetic evolution is specific among the mixed-valence cobaltites. There is no consensus so far on the structural properties of PSCO. In contrast with the *Pnma* structure of PCCO at both sides of T_{MI}, the structural symmetry of PSCO is a long-standing open question, not even yet resolved at room temperature (RT), where different orthorhombic and monoclinic space groups (like $P2_1/a$, *Imma*, $I2/a$, or $P2_1/m$) have been proposed to fit powder X-ray (and neutron) diffraction RT data.[16−20]

In recent years, there has been increasing evidence from magnetic and transverse susceptibility measurements on the magnetostructural coupling at $T_{S1} = 120$ K,[18−22] but a reliable description of the crystal structure across T_{S1} is still lacking. On the one hand, different triclinic or monoclinic symmetries have been employed to fit diffraction data at low temperatures.[16−20] On the other hand, some works attributed the magnetostructural transition to a phase separation at $T < 120$ K, suggesting a double-phase state at low temperature (e.g., $P\bar{1}$ + *Imma*). Thus, the second magnetic transition was attributed to a different orientation of the FM moment in the coexisting triclinic and orthorhombic structural phases at low temperatures.[17,18] Changes in the magnetocrystalline anisotropy are expected to be caused by modification of the structure.

Additionally, Troyanchuk et al.[16] and later Leighton et al.[19] emphasized the possible relevance of Pr 4f–O 2p hybridization for the occurrence of intriguing structural and magnetic changes around 120 K in PSCO. Let us note that neither have been observed when praseodymium is substituted by

Received: June 17, 2014
Published: November 10, 2014

other lanthanides. In particular, the critical temperature of the magnetostructural transition in PSCO at T_{S1} = 120 K is progressively lowered with diminishing praseodymium content in the $(La_{1-y}Pr_y)_{0.5}Sr_{0.5}CoO_3$ system, although a small praseodymium concentration is still enough to activate the effect.[19] Accordingly, no transition is observed in $La_{1/6}Nd_{1/3}Sr_{0.50}CoO_3$,[17] having the same average ionic radius in the A site as PSCO.

To understand the puzzling properties of half-doped PSCO, first it is necessary to determine its structural properties and provide an unambiguous description of their temperature dependence. Using high-resolution neutron diffraction in this work, we have investigated the structural evolution with temperature of the PSCO cobaltite, which adopts up to three different crystalline structures below the high-temperature $Pm\bar{3}m$ cubic phase. The successive crystal symmetries found with decreasing temperature are different from those in analogous $Ln_{0.50}Sr_{0.50}CoO_3$ FM perovskites with Ln different from praseodymium. The structural changes taking place between low temperature and 450 K are thoroughly described and analyzed, particularly across the anomalous magnetostructural transition at 120 K.

II. EXPERIMENTAL DETAILS

Ceramic samples of $Pr_{0.50}Sr_{0.50}CoO_3$ (PSCO) were prepared by solid-state reaction at high temperature and under an oxygen atmosphere. High-purity Co_3O_4 and Pr_6O_{11} oxides were first dried at 1100 °C. $SrCO_3$ was heated at 850 °C and then up to 950 °C to achieve decarbonation. The precursors were then mixed up, pressed into pellets, and heated in an oxygen atmosphere at 1000 °C for 12 h, with slow cooling (60 °C/h). After grinding and pressing, the annealing procedure was repeated several times, with the last one being performed at 1170 °C (during 24 h) under oxygen flow followed by slow cooling. X-ray diffraction patterns at RT were recorded using a Siemens D-5000 diffractometer and Cu K_α radiation. Electrical-transport (using the four-probe method) and magnetization measurements were performed using a Physical Properties Measuring System and a commercial SQUID by Quantum Design. Initial characterization confirmed a well-crystallized and single-phased metallic perovskite.

For the temperature-dependent structural study, we carried out neutron diffraction experiments on the D20 diffractometer of Institute Laue-Langevin (ILL, Grenoble, France). This two-axis high-intensity diffractometer uses a high takeoff angle of 118° for the Ge(115) monochromator, and a radial oscillating collimator precedes the large-microstrip position-sensitive detector, which covers an angular range of 150°. In this range, high-resolution data as a function of the temperature were obtained by warming the sample in a cryofurnace from 15 K up to 443 K. In ramp mode, the temperature shift for individual scans was smaller than 5 K. Using a helium cryostat, additional powder neutron diffraction patterns were also recorded at fixed selected temperatures. The data were collected at the neutron wavelength λ = 1.87 Å and were analyzed with the Rietveld method using the *FULLPROF* suite of programs.[23] The neutron patterns confirmed the PSCO material to be monophasic. Refinement of the oxygen occupation factors did not detect oxygen vacancies within an estimated error of 3%. Variable oxygen occupancies did not improve the agreement factors in the neutron fits. So, the final refinements were carried out with nominal stoichiometry.

III. RESULTS AND DISCUSSION

Figure 1a shows the susceptibility and resistivity curves of our PSCO sample. In Figure 1b, we plot a $T-2\theta$ projection of the thermal evolution of the neutron-diffracted intensities in a narrow angular range. Two sharp and well-defined structural transitions separate three different crystal structures. The corresponding transition temperatures were determined as T_{S1} = 120 K and T_{S2} = 314 K. No structural change was detected at the FM Curie point $T_C \sim 230$ K.

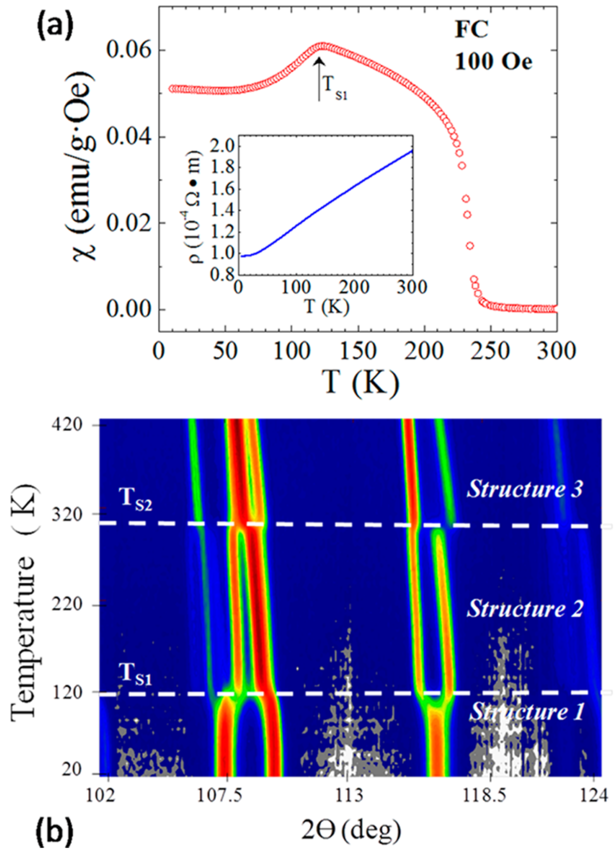

Figure 1. (a) Susceptibility of ceramic PSCO samples (field-cooled, 100 Oe). Inset: resistivity curves. (b) Neutron diffraction intensities for characteristic reflections of the successive crystal structures as a function of the temperature. Cubic $Pm\bar{3}m$ symmetry (structure 4) was reported from X-ray diffraction above 800 K.[17]

In Figure 2, we show the evolution of the reflections measured by powder neutron diffraction within the $85° < 2\theta < 90°$ interval at three representative temperatures of the three successive crystal structures. The three structures have been determined, and the continuous line in the figure corresponds to the Rietveld refinement profile calculated at each temperature. Table 1 lists the unit-cell parameters, atomic positions, isotropic thermal factors, FM moment, and reliability factors of the Rietveld refinement for each crystal structure. The measured, calculated, and difference profiles for PSCO at selected temperatures (400, 300, 150, and 15 K) are plotted in parts a–d of Figure 3, respectively.

III.a. High-Temperature Rhombohedral Phase. Diffraction data recorded between 330 and 450 K (highest temperature reached) are well reproduced by a single rhombohedral phase with space group symmetry $R\bar{3}c$ (No. 167). This symmetry corresponds to the $a^-a^-a^-$ one-tilt system in Glazer's notation[24] (a rotation of the octahedra around the 3-fold axis of the ideal cubic perovskite, a_0). The initial unit-cell parameters were taken from ref 25. The structural parameters refined at 400 K are displayed in Table 1, refering to the hexagonal axes. The hexagonal description in Table 1 corresponds to the rhombohedral structure with cell a = 5.3965 Å, α = 60.37° and atomic positions Pr/Sr at ($^1/_4$, $^1/_4$, $^1/_4$), Co at (0, 0, 0), and O at ($x + {}^1/_4$, $-x + {}^1/_4$, $^1/_4$) with x = 0.4659. Figure 3a shows the Rietveld refinement plot

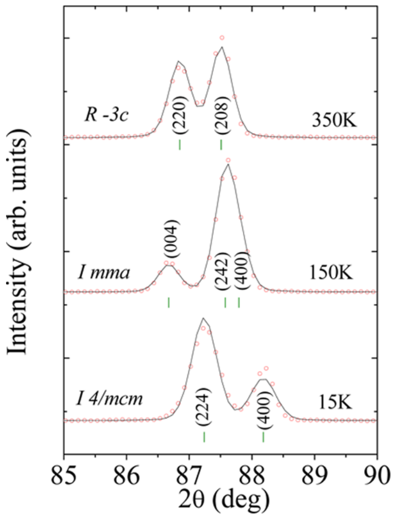

Figure 2. Selected angular region of the Rietveld refinement (solid line) of neutron patterns measured at the indicated temperatures for each structural phase. Diffraction patterns have been shifted up for clarity and are indexed according to $a_0 \times 2a_0 \times a_0$ at 150 K and $a_0 \times a_0 \times 2a_0$ at 15 K.

corresponding to this phase. Cell parameters are in good agreement with those previously reported by Balagurov et al.[17] The diffraction pattern of their PSCO sample at 773 K was still compatible with the rhombohedral symmetry, but the X-ray diffraction patterns collected at 825 K and above were attributed to the cubic $Pm\bar{3}m$ (No. 221) symmetry. Hence, the highest structural transition temperature to give a cubic $Pm\bar{3}m$ structure could be established around 800 K.[17]

III.b. Room-Temperature Orthorhombic Phase. Upon cooling below T_{S2} = 314 K, neutron patterns in the temperature range 314 K > T > 139 K are satisfactorily refined using the *Imma* (No. 74) space group, with unit-cell parameters $a \approx \sqrt{2}a_0$, $b \approx 2a_0$, and $c \approx \sqrt{2}a_0$. This symmetry perfectly reproduces the systematic absences and the neutron diffraction profiles in the mentioned range. Figure 3b shows the neutron refinement at ambient temperature (300 K). We found that at RT the rhombohedral–orthorhombic transition was already completed, and the RT diffraction pattern was single-phased (100% *Imma*). The structural details of the paramagnetic metallic orthorhombic phase at RT are given in Table 1. Figure 4a shows two projected views of the *Imma* crystal structure. In the *Imma* symmetry, there is one crystallographically independent position for Pr/Sr (4e), one for Co (4b) and two nonequivalent oxygen atoms [O1 (4e) and O2 (8g)], with three refinable coordinates: z[Pr/Sr], z[O1], and y[O2]. The tilt pattern of this orthorhombic structure corresponds to the $a^-b^0a^-$ Glazer notation (refering to the pseudocubic axes, with the long $2a_0$ axis along the b axis) as derived by Woodward.[25]

Below T_C = 230 K, the changes in the neutron experimental profile are perfectly reproduced by considering a *Imma* FM phase (see Figure 3c). The small orthorhombic distortion makes it difficult to unambiguously distinguish the exact orientation of the FM Co moments, which were aligned along

Table 1. Crystal Structures of PSCO and Reliability Factors Found by Rietveld Refinement of Neutron Data at Selected Temperatures

	400 K	300 K	150 K	15 K
space group	$R\bar{3}c$ (No. 167)	*Imma* (No. 74)	*Imma* (No. 74)	*I4/mcm* (No. 140)
a (Å)	5.4270(1)	5.3894(8)	5.3773(8)	5.3585(1)
b (Å)	5.4270(1)	7.61358(1)	7.5963(1)	5.3585(1)
c (Å)	13.1813(4)	5.43707(8)	5.4325(7)	7.7093(1)
V (Å^3)	336.207(2)	223.097(6)	221.906(5)	221.367(9)
Pr/Sr	6a	4e	4e	4b
x	0	0	0	0
y	0	0.25	0.25	0.5
z	0.25	0.0001(7)	−0.0005(4)	0.25
B (Å^2)	1.268(7)	1.129(5)	1.036(5)	0.790(6)
Co	6b	4b	4b	4c
x	0	0	0	0
y	0	0	0	0
z	0	0.5	0.5	0
B (Å^2)	0.718(5)	0.4778(9)	0.162(3)	0.459(2)
O1	18e	4e	4e	4a
x	0.466(2)	0	0	0
y	0	0.25	0.25	0
z	0.25	0.4582(7)	0.4540(6)	0.25
B (Å^2)	1.641(5)	1.164(6)	1.077(4)	1.190(1)
O2		8g	8g	8h
x		0.25	0.25	0.2849(3)
y		0.0231(4)	0.0233(2)	0.7849(3)
z		0.75	0.75	0
β		1.531(3)	1.085(4)	1.028(6)
ordered FM moment (μ_B/Co)			1.47(3)	0.84(4)
χ^2	2.06	1.08	1.63	2.38
R_B (%)	2.89	3.15	2.47	2.39
R_{mag} (%)			6.17	7.2

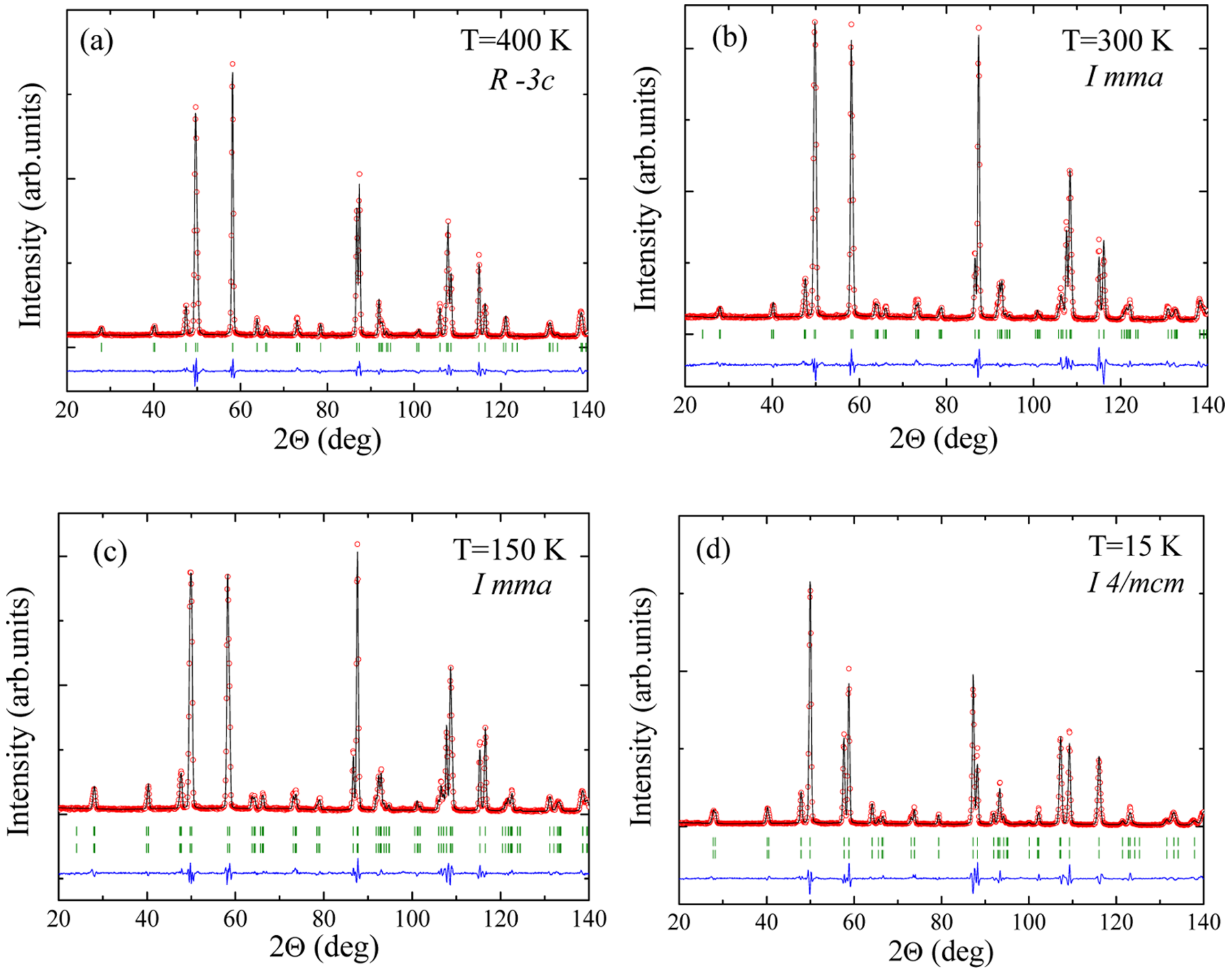

Figure 3. Rietveld refinement (black line) of neutron diffraction patterns [red circles, experimental points; bottom blue line, difference (bottom)] for PSCO at selected temperatures: (a) 400 K, rhombohedral $R\bar{3}c$ structure; (b) 300 K, orthorhombic *Imma* paramagnetic phase; (c) 150 K, orthorhombic *Imma* FM phase (the second row of Bragg positions is the magnetic phase); (d) 15 K, tetragonal *I*4/*mcm* phase.

the y axis in the fit. The ordered FM moment in the *Imma* phase (1.5 μ_B/Co at 150 K) is not compatible with Co^{3+} and Co^{4+} species, both in a high-spin (HS) configuration. Instead, a mixture of Co^{3+} ions in the IS (LS) configuration coexisting with Co^{4+} species in a LS (IS) state seems more likely. The unit-cell parameters, atomic positions, isotropic thermal factors, FM moment, and reliability factors obtained at 150 K are listed in Table 1. This temperature is above but very close to the phase transition at T_{S1} = 120 K.

III.c. Low-Temperature Tetragonal Structure. There is no phase separation at low temperature. Instead, the neutron patterns below 120 K are well described using a single tetragonal phase, *I*4/*mcm* (No. 140) space group. In the *I*4/*mcm* structure, the number of free atomic coordinates reduces to one: Co is at the 4c site (0 0 0), Pr/Sr at the 4b position (0, $^1/_2$, $^1/_4$), and O1 at 4a (0, 0, $^1/_4$) and O2 occupies the 8h site (x, x + $^1/_2$, 0), with $x \approx 0.2849$. By testing the monoclinic *I*2/*a* symmetry proposed in ref 19 (maximal subgroup of *Imma*) against our neutron data for $T < T_{S1}$, we confirmed that the refined solution plainly converges, approaching the tetragonal description given in Table 1. Analogously, we confirmed that common subgroups of *Imma* in perovskites and other related symmetries like *I*2/*m*, $P2_1/n$, *Cmmm*, *Fmmm* ($2a_0 \times 2a_0 \times 2a_0$) observed in similar manganites do not apply here. We recall that an *I*4/*mcm* → *Imma* transition was reported at 430 K by electron microscopy data in $Pr_{0.5}Sr_{0.5}MnO_3$.[26]

Neutron patterns in the low-temperature phase did not show any reflection from an antiferromagnetic multiple cell. As indicated by the low-field magnetization, we only observed a reduction of the FM intensity at the orthorhombic−tetragonal transition. The refined ordered FM moment rapidly drops from 1.5 to 0.8 μ_B/Co. At low temperature, the R_{mag} agreement factor could suggest m_x moments (R_{mag} = 7.70; R_B = 2.38) rather than m_z ones (R_{mag} =7.88; R_B = 2.69). Figure 3d illustrates the agreement between observed and calculated profiles at 15 K (former model; see also Table 1). Selected interatomic distances and bond angles are given in Table 2.

III.d. Structural Changes in PSCO. The structural transformations in PSCO noticeably differ from those in $Ln_{0.5}Sr_{0.5}CoO_3$ perovskites. With decreasing temperature, successive distortions reduce the ideal perovskite cubic symmetry following the $Pm\bar{3}m$ → $R\bar{3}c$ → *Imma* → *I*4/*mcm* sequence. In Glazer notation (refering to the pseudocubic axes), the successive tilt systems, as derived by Woodward,[25] are $a^0a^0a^0 \rightarrow a^-a^-a^- \rightarrow a^-b^0a^- \rightarrow a^0a^0c^-$. Notice that the orthorhombic cell corresponds to $\sqrt{2}a_0 \times 2a_0 \times \sqrt{2}a_0$, whereas the tetragonal is $\sqrt{2}a_0 \times \sqrt{2}a_0 \times 2a_0$ (a_0: cubic) in

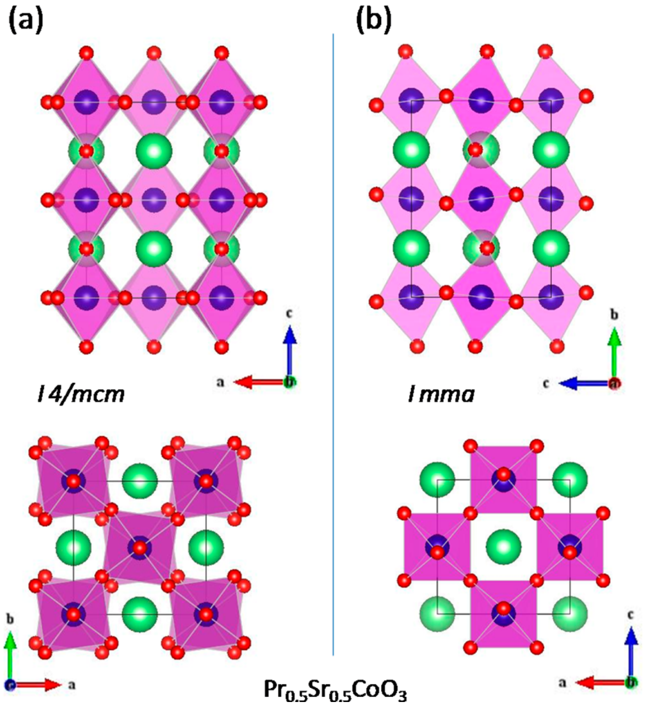

Figure 4. Projections of (a) the tetragonal *I*4/*mcm* crystal structure refined at 15 K and (b) the orthorhombic *Imma* structure of PSCO at 300 K. Color code: green balls, Pr and Sr ions; blue balls, Co atoms; red balls, O atoms.

Table 1. To gain clarity, the *Imma* symmetry can also be described in the *Ibmm* setting (the setting of the tetragonal cell: $\sqrt{2}a_0 \times \sqrt{2}a_0 \times 2a_0$, long vertical *c* axis), for which the tilts (referred to the pseudocubic axes) are $a^-a^-c^0$. This setting is more convenient for comparison with the tetragonal phase. Hence, the changes between two successive octahedral tilt patterns are easily visualized, and the final sequence results $a^0a^0a^0 \rightarrow a^-a^-a^- \rightarrow a^-a^-c^0 \rightarrow a^0a^0c^-$. Therefore, in the $R\bar{3}c \rightarrow$ *Imma* transition the rotation around the vertical pseudocubic axis has been suppressed. Moreover, the orthorhombic tilting of the octahedra in antiphase along *a* and *b* pseudocubic axes is suppressed at the *Imma* → *I*4/*mcm* transition, whereas the tilting around the vertical axis is activated in antiphase for successive octahedra along the *c* axis sharing an apical oxygen. These two crystal structures have been represented and are compared in Figure 4.

Analysis of the neutron patterns recorded by varying the temperature allows us to monitor the structural changes at T_{S1} and T_{S2}. Figure 5a plots the temperature evolution of the cell volume up to 450 K. The V_0 volume per formula unit allows one to obtain the a_0 reference parameter ($a_0 = V_0^{1/3}$). The experimental V_0 values were fitted to

$$V_0 = V_1 + V_2\Theta \coth(\Theta/T) \quad (1)$$

in the whole temperature interval up to 450 K (continuous line in Figure 5a). The Θ temperature accounts for the saturation effects in the thermal contraction as *T* approaches 0 K.[27] The volume contraction at the *Imma* → *I*4/*mcm* transition in PSCO

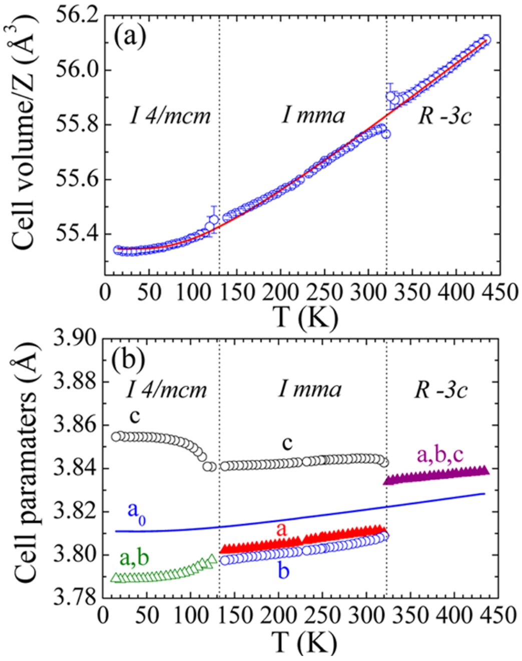

Figure 5. (a) Evolution of the cell volume (per formula unit, *Z*) up to 450 K. The solid line, fitting the equation $V_0 = V_1 + V_2\Theta \coth(\Theta/T)$, is a guide to the eye. (b) Evolution of the reduced lattice parameters with temperature. The solid line shows the reference parameter a_0 obtained from the reduced volume ($a_0 = V_0^{1/3}$) .

Table 2. Evolution of Main Interatomic Distances and Bonding Angles in the Successive Phases of PSCO

	400 K, $R\bar{3}c$	300 K, *Imma*	150 K, *Imma*	15 K, *I*4/*mcm*	relative variation (15−150 K), %
$d_{\text{Co−O1}}$ (Å) ×2	1.922(13)	1.917(3)	1.915(4)	1.927(3)	0.6
$d_{\text{Co−O2}}$ (Å) ×4	1.922(13)	1.922(4)	1.919(2)	1.913(6)	−0.3
$\langle d_{\text{Co−O}}\rangle$ (Å)	1.922(13)	1.919(4)	1.918(3)	1.920(5)	0.1
Co−O1−Co (deg)	168.92(8)	166.38(16)	165.00(15)	180.00(4)	8.3
Co−O2−Co (deg)	168.92(8)	169.50(6)	169.41(2)	164.11(2)	−3.2
⟨Co−O−Co⟩ (deg)	168.92(8)	168.46(11)	167.94(9)	169.41(3)	0.9
R−O1 (Å)	2.899(16)	2.946(4)	2.963(15)	2.679(5)	−10.6
R−O1 (Å)	2.528(16)	2.491(4)	2.469(15)	2.679(5)	7.8
R−O1 (Å) ×2	2.705(13)	2.704(3)	2.700(3)	2.679(5)	−0.8
⟨R−O1⟩ (Å)	2.709(15)	2.711(4)	2.711(11)	2.679(5)	−1.2
R−O2 (Å) ×2	2.528(16)	2.579(16)	2.571(14)	2.524(14)	−1.9
R−O2 (Å) ×2	2.899(16)	2.828(18)	2.822(13)	2.524(14)	−11.8
R−O2 (Å) ×2	2.705(13)	2.828(18)	2.822(13)	2.894(13)	2.5
R−O2 (Å) ×2	2.705(13)	2.579(16)	2.571(14)	2.894(13)	11.2
⟨R−O2⟩ (Å)	2.709(15)	2.702(17)	2.697(14)	2.709(13)	0.4

is rather small (0.1%) compared to the 2% volume contraction in PCCO at the *Pnma* → *Pnma* transition when it enters the insulating phase.[9]

Figure 5b shows variation of the unit-cell parameters for PSCO across the two structural transitions between 15 and 450 K. The reduced lattice parameters facilitate the comparison between structures, and the solid line in the plot represents the reference parameter a_0 ($a_0 = V_0^{1/3}$) obtained from the fit of the reduced volume. The abrupt anisotropic changes observed at the first [from $R\bar{3}c$ ($a^-a^-a^-$) to *Imma* ($a^-a^-c^0$)] and second [from *Imma* ($a^-a^-c^0$) to *I*4/*mcm* ($a^0a^0c^-$)] transitions are both indicative of discontinuous phase transitions.

In the orthorhombic phase, the CoO_6 octahedra remain close to regular (d_{apical}/d_{basal} = 1.917 Å/1.922 Å and d_{Co-O} = 1.919 Å at RT). Moreover, the bond-angle distortion in the plane between corner-sharing octahedra within the *a*−*c* plane is slightly lower but very similar to that between adjacent octahedra along the *b* axis (RT values: Co−O2−Co = 169.4° vs Co−O1−Co = 166.4°). As a consequence, the mobility of conducting charges is expected to be very isotropic.

There is a marked enlargement across T_{S1} of the Co−O1−Co distance between octahedra sharing apical oxygen atoms: parameter *b* = 7.596 Å in the *Imma* phase transforms to *b* = 7.709 Å in the *I*4/*mcm* structure (i.e., +1.5% variation). There are two main causes for expansion of the *c* lattice parameter in the tetragonal phase: the straightening of the Co−O1−Co bond angle (θ_1) and a stretching deformation in the octahedron (Table 2 and Figure 6). The Co−O1−Co bond angle θ_1 increases 15° at the transition up to the ideal 180° in the tetragonal phase (see Figure 6a, so that the *a* tilts in the orthorhombic $a^-a^-c^0$ system vanish to adopt the $a^0a^0c^-$ configuration. In the low-temperature phase, the alternating rotations of the octahedra around the tetragonal *c* axis are plotted in Figure 4a. From θ_2 (Co−O2−Co) values in Table 2, the in-plane tilt angles, $\phi_2 = 1/2[180° - \theta_2]$, make ±7.95°.

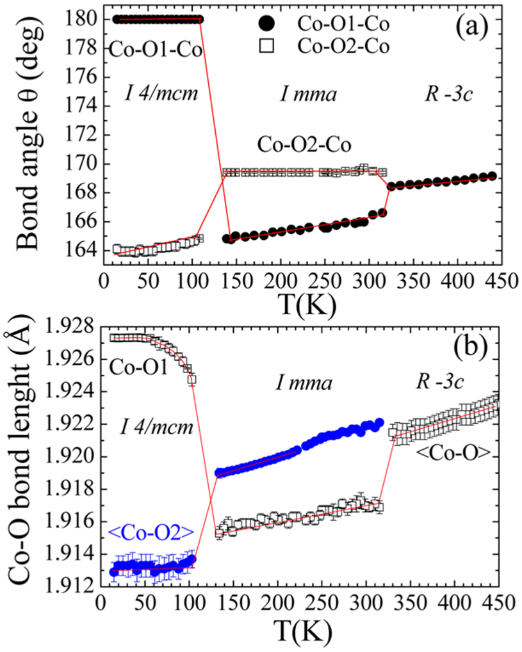

Figure 6. (a) Evolution with temperature of the Co−O−Co bond angles. (b) Evolution of the average Co−O1 and Co−O2 bond lengths in the CoO_6 octahedra across the structural phase transitions.

On the other hand, as shown in Table 2, there is a stretching deformation of the CoO_6 octahedra at the orthorhombic−tetragonal transition. The d_{Co-O1}/d_{Co-O2} ratio found above T_{S1} (0.9980 at 150 K) reaches 1.0075 at 15 K. The temperature dependence of the basal and apical Co−O bond lengths in the average CoO_6 octahedron of PSCO is depicted in Figure 6b. Evolution of the two characteristic metal−oxygen bonds shown in Figure 6b qualitatively mimics the trend of the cell parameter size across the two structural transitions represented in Figure 5b.

The apical Co−O1 bond suddenly enlarges at T_{S1} upon cooling. This expansion entering the tetragonal phase (0.62%) is closely twice the contraction observed in each one of the two Co−O2 basal bonds (0.32%). Consequently, the elongation observed along the tetragonal axis during the orthorhombic−tetragonal symmetry change takes place without practically varying the inner volume in the octahedron. Despite the fact that evolution of the ⟨Co−O⟩ bond length across the MIT in PCCO is very similar to the evolution observed in PSCO across T_{S1} (see the inset of Figure 7b), the deformation of the regular octahedron was not observed in the calcium-based compound.[9] Let us recall that, although the volume of the octahedron does not significantly change in PCCO perovskite, synchrotron X-ray spectroscopic techniques proved sudden spin-state changes in Co^{3+} ions at the MIT of the *Pnma* calcium-based perovskite.[14]

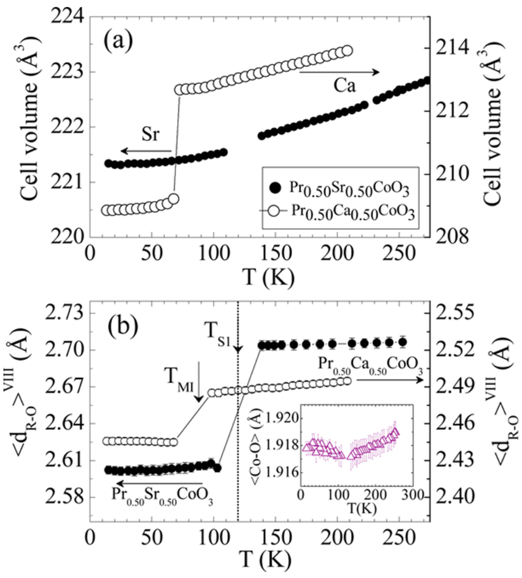

Figure 7. Comparative evolution of (a) the cell volume and (b) the average (Pr, A)−O interatomic distance (VIII shell, A = Ca or Sr) of PSCO (left axis) and PCCO (right axis). The inset in panel b depicts the average Co−O distance in PSCO.

Evolution below 200 K of the unit-cell volume of metallic PSCO is compared in Figure 7a to that of the PCCO (data from ref 9). The plot shows that the cell volume contraction in PSCO at T_{S1} is very small (0.1%) compared to the 2% volume contraction in PCCO at the MIT. In both cases, the volume reduction is not due to changes in the volume of the octahedra but mainly to changes in the R−O bond lengths [R = Pr, A with A = Sr or Ca]. To be noticed here is that at T_{S1} the contraction in mostly R−O bond lengths of the first eight nearest-neighbor oxygen atoms around the R site (VIII shell) at T_{S1} in PSCO is relatively larger than that in PCCO at T_{MI} (see

Table 2 for Sr and ref 12 for calcium samples). Nevertheless, given the insignificant changes in the volume of the octahedra, Figure 7a shows that the reduction of the Pr/A polyhedral volume is around one order of magnitude smaller in PSCO than in PCCO. In the tetragonal phase, there are only three distinct Pr−O distances versus five in the orthorhombic structure. At low temperature, praseodymium atoms (at the R site) are coordinated by 8 + 4 oxygen atoms. For comparison purposes between different phases and samples, we include in the VIII shell the shortest bonds to the first four O2 and O1 atoms, respectively. In Figure 8, we have plotted the temperature evolution of all individual R−O bond lengths in PSCO in the 15−450 K range. Figure 7b shows the low-temperature evolution of the average $\langle R{-}O\rangle^{VIII}$ interatomic distance for PSCO and PCCO cobaltites. Despite the small volume contraction at T_{S1}, Figure 7b illustrates that there is a strong shortening of the average $\langle R{-}O\rangle^{VIII}$ bond length in PSCO at T_{S1}. In fact, the change observed in $\langle (Pr, Sr){-}O\rangle^{VIII}$ (∼−4%) is around twice the size of the average bond contraction in PCCO across the MIT, where a Pr^{3+} to Pr^{4+} valence drift produces the Pr−O bond shortening.[11−13] If one applies the phenomenological Brown's bond valence model[28,29] to the R−O distances in Table 2, the resulting valence associated with the Pr−O bonds in the VIII shell changes from +2.12 at 150 K up to +2.92 in the tetragonal phase.[30] Also, the total valence associated with the four outer Pr−O2 bonds decreases from +0.99 to +0.27 upon cooling across the $Imma \rightarrow I4/mcm$ transition.

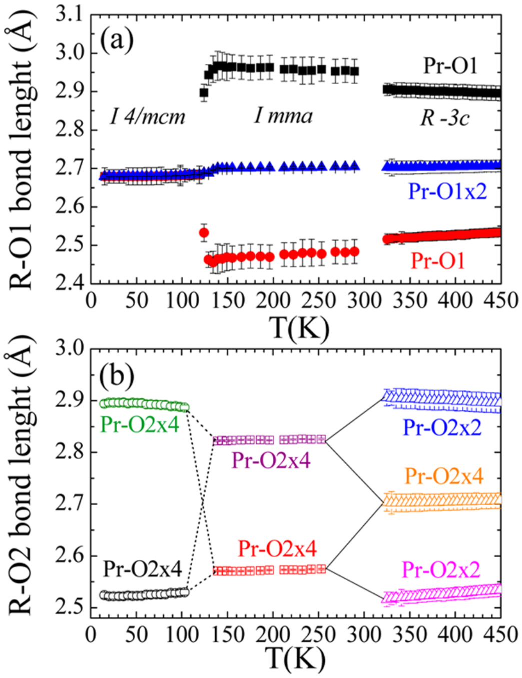

Figure 8. Evolution of the (a) R−O1 and (b) R−O2 bond lengths in PSCO in the rhombohedral, orthorhombic, and tetragonal phases and across the structural transitions.

IV. CONCLUSIONS

Among the FM/metallic $Ln_{0.50}Sr_{0.50}CoO_3$ compounds, the PSCO system exhibits unique structural and magnetic features. Two successive magnetic transitions contrast with the single FM transition of cobalt moments in other $Ln_{0.50}Sr_{0.50}CoO_3$ compounds. Although the intriguing transition at $T_{S1} \sim 120$ K, characterized by a steplike behavior in the magnetization, had been ascribed to changes in the magnetocrystalline anisotropy, the structural evolution of the praseodymium-based half-doped cobaltite has been the object of a long-standing controversy.

In this work, we have determined and described evolution of the PSCO crystal structure from low temperature up to 450 K. The deviation from the ideal cubic structure with decreasing temperature follows the transformation $Pm\bar{3}m \rightarrow R\bar{3}c \rightarrow Imma \rightarrow I4/mcm$. It thus differs from the structural behavior of parent compounds with Ln ≠ Pr [such as $Nd_{0.5}Sr_{0.5}CoO_3$, $(La_{1/3}Nd_{2/3})_{0.50}Sr_{0.50}CoO_3$, or $La_{0.5}Sr_{0.5}CoO_3$].

Magnetostructural effects induced by the $Imma \rightarrow I4/mcm$ symmetry change are responsible for the second magnetic transition and the so-called "two-step magnetic evolution" in PSCO. Magnetic evolution in the powder neutron diffraction data (which show FM intensity) is compatible with a modification of the FM easy axis and confirms a reduction of the ordered FM moment at the transition. The compound is single phased at low temperature, and the possibility of a phase separation phenomena previously proposed to explain anomalous magnetostructural evolution across the T_{S1} transition must be ruled out.

This magnetostructural transition has not been reported in any other $Ln_{0.50}Sr_{0.50}CoO_3$ perovskite not containing praseodymium. The changes observed around praseodymium atoms have been compared to changes reported in PCCO, where an active participation of Pr 4f electrons at the metal−insulator transition was unexpectedly reported. Even though there is a strong shortening of the average $\langle R{-}O\rangle^{VIII}$ bond length in PSCO at T_{S1} (−4%, twice the size of the average contraction in PCCO), bond valence estimations do not require the appearance of the Pr^{4+} oxidation state. A deeper analysis of this cobaltite requires further experimental work using additional techniques, which must also clarify whether the presence of praseodymium is playing or not an active role. The tetragonal symmetry found in the low-temperature phase requires a very homogeneous and symmetric distribution of praseodymium bonding electrons among, separately, the different Pr−O1 and Pr−O2 bonds, in contrast with the large dispersion of Pr−O bond lengths in the orthorhombic I-centered phase. Although the volume of individual CoO_6 octahedra is hardly modified in the transition, they undergo a remarkable elongation along its tetragonal axis, compatible with an orbital ordering in Co^{3+} centers having an IS state. In spite of the orthorhombic ($a^-a^-c^0$) to tetragonal ($a^0a^0c^-$) transformation, the PSCO system preserves the metallic character, but a significant reorganization of the conducting bands is anticipated from the loss of isotropy in the reported low-temperature crystal structure. Likewise, the structural changes imply strong modifications in the strength of the double-exchange coupling along the different directions. A deeper understanding of this cobaltite requires further diffraction and absorption experimental and theoretical work on powder and/or single crystals and under the application of magnetic field, which must clarify whether the presence of praseodymium is playing or not an active role and the implications of the described structural changes on the peculiar magnetic behavior.

■ AUTHOR INFORMATION

Corresponding Author

*E-mail: garcia.munoz@icmab.es.

Notes

The authors declare no competing financial interest.

ACKNOWLEDGMENTS

We are thankful for financial support from MINECO (Spanish government) under Projects MAT2009-09308, MAT2012-38213-C02-02, and CSD2007-00041 (NANOSELECT) and to the ILL for granting beamtime. C. Ritter is acknowledged for technical assistance during neutron measurements. J.P.-P. thanks the CSIC for a JAE-Pre contract.

REFERENCES

(1) Goodenough, J. B. *J. Phys. Chem. Solids* **1958**, *6*, 287.
(2) Raccah, P. M.; Goodenough, J. B. *Phys. Rev. B* **1967**, *155*, 932–943.
(3) Señarís-Rodríguez, M. A.; Goodenough, J. B. *J. Solid State Chem.* **1995**, *116*, 224–231.
(4) Saitoh, T.; Mizokawa, T.; Fujimori, A.; Abbate, M.; Takeda, Y.; Takano, M. *Phys. Rev. B* **1997**, *55*, 4257–4266.
(5) Troyanchuk, I. O.; Kasper, N. V.; Khalyavin, D. D.; Szymczak, H.; Szymczak, R.; Baran, M. *Phys. Rev. Lett.* **1998**, *80*, 3380–3383.
(6) Frontera, C.; García-Muñoz, J. L.; Llobet, A.; Aranda, M. A. G. *Phys. Rev. B* **2002**, *65*, No. 180405R.
(7) Maignan, A.; Caignaert, V.; Raveau, B.; Khomskii, D.; Sawatzky, G. *Phys. Rev. Lett.* **2004**, *93*, No. 026401.
(8) Tsubouchi, S.; Kyômen, T.; Itoh, M.; Ganguly, P.; Oguni, M.; Shimojo, Y.; Morii, Y.; Ishii, Y. *Phys. Rev. B* **2002**, *66*, No. 052418.
(9) Barón-González, A. J.; Frontera, C.; García-Muñoz, J. L.; Blasco, J.; Ritter, C. *Phys. Rev. B* **2010**, *81*, No. 054427.
(10) Hejtmánek, J.; Šantavá, E.; Knížek, K.; Maryško, M.; Jirák, Z.; Naito, T.; Sasaki, H.; Fujishiro, H. *Phys. Rev. B* **2010**, *82*, No. 165107.
(11) Knížek, K.; Hejtmánek, J.; Novák, P.; Jirák, Z. *Phys. Rev. B* **2010**, *81*, No. 155113.
(12) García-Muñoz, J. L.; Frontera, C.; Barón-González, A. J.; Valencia, S.; Blasco, J.; Feyerherm, R.; Dudzik, E.; Abrudan, R.; Radu, F. *Phys. Rev. B* **2011**, *84*, No. 045104.
(13) Herrero-Martín, J.; García-Muñoz, J. L.; Valencia, S.; Frontera, C.; Blasco, J.; Barón-González, A. J.; Subías, G.; Abrudan, R.; Radu, F.; Dudzik, E.; Feyerherm, R. *Phys. Rev. B* **2011**, *84*, No. 115131.
(14) Herrero-Martín, J.; García-Muñoz, J. L.; Kvashnina, K.; Gallo, E.; Subías, G.; Alonso, J. A.; Barón-González, A. J. *Phys. Rev. B* **2012**, *86*, No. 125106.
(15) Mahendiran, R.; Schiffer, P. *Phys. Rev. B* **2003**, *68*, No. 024427.
(16) Troyanchuk, I. O.; Karpinskii, D. V.; Chobot, A. N.; Voitsekhovich, D. G.; Bobryanskii, V. M. *JETP Lett.* **2006**, *84*, 151–155.
(17) Balagurov, A. M.; Bobrikov, I. A.; Karpinsky, D. V.; Troyanchuk, I. O.; Pomjakushin, V. Y.; Sheptyakov, D. V. *JETP Lett.* **2008**, *88*, 531–536.
(18) Balagurov, A. M.; Bobrikov, I. A.; Pomjakushin, V. Y.; Pomjakushina, E. V.; Sheptyakov, D. V.; Troyanchuk, I. O. *JETP Lett.* **2011**, *93*, 263–268.
(19) Leighton, C.; Stauffer, D. D.; Huang, Q.; Ren, Y.; El-Khatib, S.; Torija, M. A.; Wu, J.; Lynn, J. W.; Wang, L.; Frey, N. A.; Srikanth, H.; Davies, J. E.; Liu, K.; Mitchell, J. F. *Phys. Rev. B* **2009**, *79*, No. 214420.
(20) Li, F.; Wu, N.; Fang, J. *J. Supercond. Novel Magn.* **2013**, *26*, 463–467.
(21) Frey Huls, N. A.; Bingham, N. S.; Phan, M. H.; Srikanth, H.; Stauffer, D. D.; Leighton, C. *Phys. Rev. B* **2011**, *83*, No. 024406.
(22) Hirahara, S.; Nakai, Y.; Miyoshi, K.; Fujiwara, K.; Takeuchi, J. *J. Magn. Magn. Mater.* **2007**, *310*, 1866–1867.
(23) Rodríguez-Carvajal, J. *Physica B* **1993**, *192*, 55–69.
(24) Glazer, A. M. *Acta Crystallogr.* **1972**, *B28*, 3384–3392.
(25) Woodward, P. M. *Acta Crystallogr.* **1997**, *B53*, 32–43.
(26) Damay, F.; Martin, C.; Hervieu, M.; Maignan, A.; Raveau, B.; Andre, G.; Bouree, F. *J. Magn. Magn. Mater.* **1998**, *184*, 71–82.
(27) Tan, T.-Y.; et al. *Phys. Rev. B* **2012**, *85*, No. 104107.
(28) Brese, N. E.; O'Keefe, M. *Acta Crystallogr.* **1991**, *B47*, 192–197.
(29) Brown, I. D. *Z. Kristallogr.* **1992**, *199*, 255–272.
(30) Shannon, R. D. *Acta Crystallogr.* **1976**, *A32*, 751–767 From this report, the reference value $d(\mathrm{Sr{-}O})^{\mathrm{VIII}}$= 2.66 Å for the Sr–O distance was assumed in the estimation of the valence.